



On Processing of Waste Polyethylene Terephthalate Glycol for Sensory Applications

Kanwerajit Singh¹ · Rupinder Singh² · Amrinder Pal Singh¹

Received: 6 March 2024 / Accepted: 7 July 2024
© The Institution of Engineers (India) 2024

Abstract

Owing to its various advantages, polyethylene terephthalate glycol (PETG) has been employed in a broad spectrum of applications, including the packing of foodstuff, biomedical devices, containers, 3D printing, etc., which has led to it being a contributor to waste (both domestic and commercial). Several studies have recently been reported on PETG waste recycling, but little has been reported on processing PETG waste for sensory applications. This study highlights the processing of waste PETG for 3D printing of sensors supported by mechanical, thermal, rheological, and mechanical characterization. The process started with collecting waste PETG, mechanical segregation, crushing, and melting at 250 °C. To ensure recyclability for sensor fabrication, mechanical, rheological, thermal, Fourier transmission infrared spectroscopy (FTIR), and scanning electron microscopy (SEM) analysis were performed. The results suggest that Young's modulus (E) increased by 42.8% from 0.586 GPa to 0.737 GPa, and porosity decreased from 26.54 to 19.19% in 04 processing cycles. No considerable change in the glass transition temperature (T_g) was noticed, and the flowability of PETG was increased by 186.98% in 04 processing cycles. A continuous decrease in the absorption intensity of C=O at wave number (WN) 1700 cm⁻¹ has been observed in recycled PETG. For sensory applications, the resistance of recycled PETG was increased in every processing cycle, which may be suitable for ascertaining the change in the charge-carrying capacity of the materials. Finally, after the fourth cycle, a 113.29% increase was observed.

Keywords PETG · Recycling · Mechanical · Thermal · Morphological properties · Sensors

Introduction

PETG (C₁₄H₂₀O₅S) is the improved thermoplastic version of polyethylene terephthalate (PET), produced by copolymerizing with glycol, which enhances the material's flexibility, formability, and impact strength compared to PET [1]. PETG is one of the most suitable polymers for 3D printing because of its good layer adhesion and minimal warping [2]. It is used for functional prototypes, mechanical parts, and end-use products. Its electrical insulation, chemical, and moisture-resistant properties make it a suitable candidate

for electronic and electrical applications such as substrate material for sensors, electrical enclosures, circuit board components, and cable insulations [3]. PETG is widely used in the packaging industry as it is a food-grade material that is durable, safe at elevated temperatures, chemically resistant, transparent, and tough, and it can bear the impact load. Generally, it is used for food containers, clamshell packing, cosmetic packing, blister packs, display cases, hot-fill containers, etc. [4–7]. Due to its optical clarity and excellent light transmission, it is used for signage, point-of-sale displays, retail fixtures, exhibition stands, etc. [3]. Automotive parts such as light covers, door panels, instrument clusters, grille inserts, interior trim, etc., are manufactured using PETG because of the resistance to impact loading and weatherability. Many of these are 3D-printed parts [8]. Medical and dental equipment comprises PETG because of its biocompatibility [9, 10] and ease of sterilization. Some are trays, housings, instrument handles, and dental retainers. PETG has also been used in tissue engineering [10]. PETG is ideal for protective equipment like face shields, safety goggles,

✉ Rupinder Singh
rupindersingh@nitttrchd.ac.in

¹ Mechanical Engineering Department, University Institute of Engineering and Technology, Panjab University, Chandigarh, India

² Mechanical Engineering Department, National Institute of Technical Teacher Training and Research, Chandigarh, India

visors, and helmets. It is a non-biodegradable polymer made from petroleum-based sources. Supports made of PETG in 3D printing are removed to get the desired product, leading to PETG being wasted. Trimming and scraping during packaging and signage contribute to the wastage of PETG. While manufacturing and processing, the unusable and unsuitable material is discarded as pellets, flakes, or regrind material. Hence, the wastage from the abovementioned applications leads to high volumes of non-biodegradable waste. PETG products' post-consumer waste is enormous [11], and significant recycling efforts are required. Commercially, waste material is collected from post-consumer products and sorted to get the necessary material. The collected material is shredded into small pieces and cleaned using warm water. After cleaning, PETG flakes are dried to remove moisture. Dried PETG is melted and forced to pass through a small opening to form thin strands or filaments. Then, this recycled material is used to manufacture a product using injection moulding, 3D printing, etc. [12].

The literature reveals that owing to its various advantages, PETG has been employed in a broad spectrum of applications, including the packing of foodstuff, biomedical devices, containers, 3D printing, etc., which has led to it contributing to waste (both domestic and commercial) [12–14]. Several studies have recently been reported on PETG waste recycling [15], but little has been reported on processing PETG waste for sensory applications. This study highlights the processing of waste PETG for 3D printing of sensors supported by mechanical, thermal, rheological, and mechanical characterization.

Materials and Methods

Figure 1 shows the methodology adopted in this study.

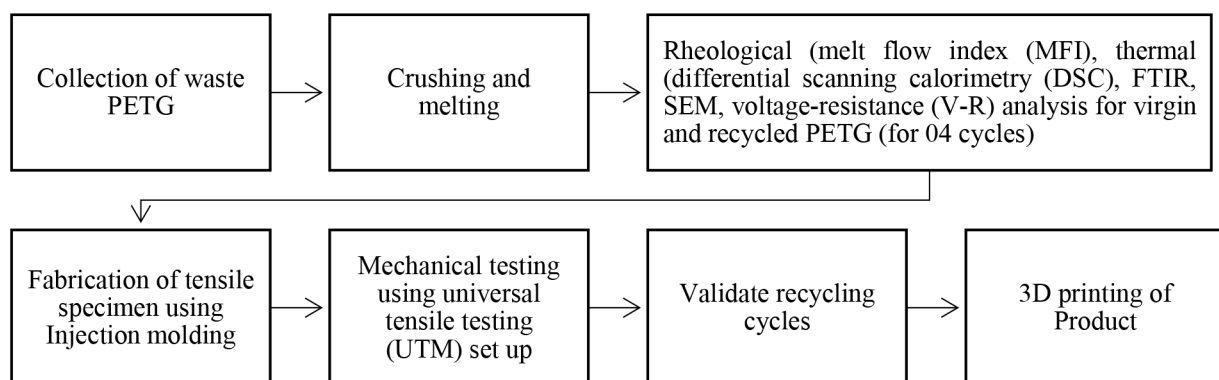


Fig. 1 Methodology adopted

Collection of Waste Material

Post-consumer waste of PETG bottles from various medical research labs was collected. These bottles are used to store media for cell culture. This media comprises amino acids, vitamins, inorganic salts, glucose, and serum. The cells grown in this media are used in the In-Vitro analysis.

Crushing and Melting

Unwanted material from the bottles, like tags, labels, etc., was removed. Bottles were crushed and shredded as per the reported study [16]. These crushed bottles were then exposed to high temperatures, i.e., 250 °C, and melted to form pellets for virgin PETG. These pellets were remelted and processed for four recycling cycles.

Melt Flow Index (MFI)

The MFI of virgin and recycled PETG has been evaluated according to ASTM D1238. It measures the quantity of molten material in (g) coming out in 10 min by putting 2.16 kg weight [17, 18]. This process was performed twice, and a mean MFI of the samples was calculated for virgin and four recycling cycles to minimize the experimental error.

DSC Analysis

A thermoanalytical technique DSC has been used to determine the T_g and effect of recyclability on the thermal properties of the PETG material. This analysis has been performed in 3 cycles. A cycle consists of heating material from 0 to 300 °C and cooling it to 0 °C at 10 °C/min with an airflow rate of 50 ml/min. In the first cycle, it is assumed that the pre-history of the material is removed, and the data of the other two cycles has been considered for the analysis [19, 20]. The study was performed on virgin and recycled PETG (processed for four recycling cycles).

FTIR Analysis

The molecular vibrations in the sample to absorb/transmit the incident infrared radiation (IR) corresponding to a specific wavenumber were ascertained. The IR spectrum was categorized into three distinct wavenumber ranges: the far-IR spectrum (below 400 cm^{-1}), the mid-IR spectrum (ranging from 400 to 4000 cm^{-1}), and the near-IR spectrum (ranging from 4000 to $13,000\text{ cm}^{-1}$) [21]. This study used the mid-IR spectrum for virgin and recycled PETG.

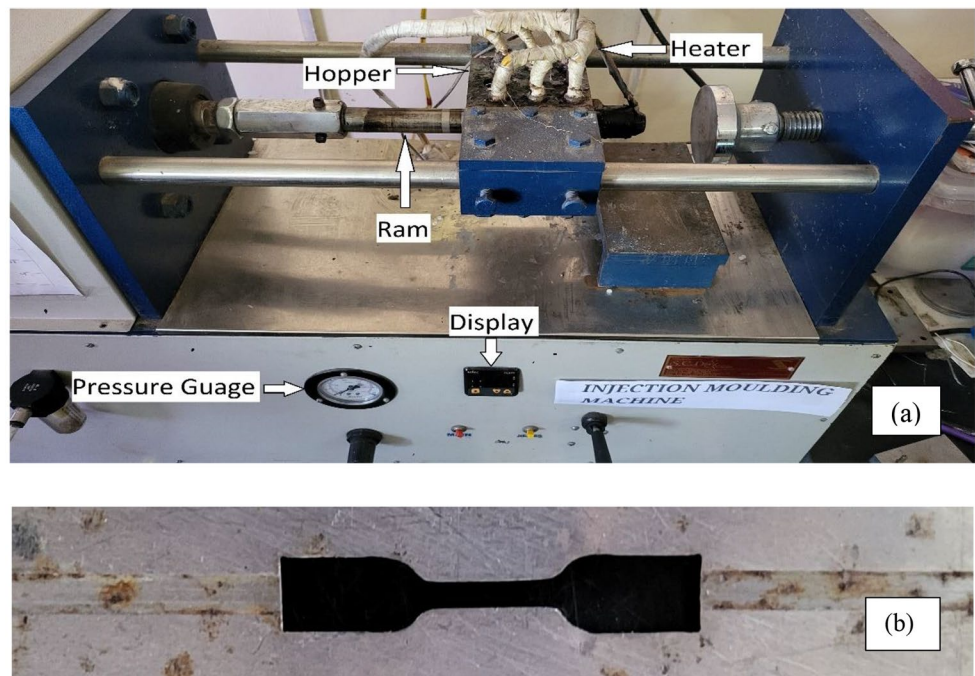
V-R Analysis

The source measure unit (SMU) was used to explore the resistance behaviour of the virgin and recycled PETG. SMU is a specialized device capable of accurately delivering voltage/current while measuring current/voltage. It integrates the functionalities of a digital multimeter, electronic load, accurate current source, and pulse generator into a single compact instrument with tight synchronization. The experiment was conducted in a dark room with uniform surroundings for comparative studies.

Injection Molding

For the mechanical characterization of the PETG polymer, a tensile specimen (as per ASTM D638, Type V) [18] has been fabricated using an injection moulding machine. The temperature was kept at $245\text{ }^{\circ}\text{C}$, and the pressure was in the 6 to 8 bar range. Figure 2a and b show the injection moulding setup used in this study and the prepared tensile

Fig. 2 (a) Injection moulding set up, (b) Tensile specimen



specimen. It has been observed that with the increase in MFI, the injection dwell and cooling time of the injection moulding decreases, further reducing the operation time.

UTM

Mechanical properties of the material have been calculated using a UTM with 400 N capacity (Fig. 3). The prepared tensile specimen has been jogged into the machine, and at a rate of 10 mm/s , both ends of the specimen have been pulled to calculate the E of PETG specimens [17].

SEM Images and Porosity (%)

Fractured samples, which were used to evaluate E, were examined using SEM. The voltage of 3 kV was used to direct an electron beam at the fractured site to capture the image at $\times 100$ magnification. These images of SEM were further used in metallurgical image analysis software (MIAS) to find the porosity percentage (as per ASTM B 276) at the fractured sites.

Results and Discussion

Table 1 shows observations for MFI in different processing cycles.

It has been observed from Table 1 that the MFI was increased with the recycling cycles, which may be due to breakage of polymer chains (due to mechanical and thermal stresses) in repeated cycles, resulting in shortening of the

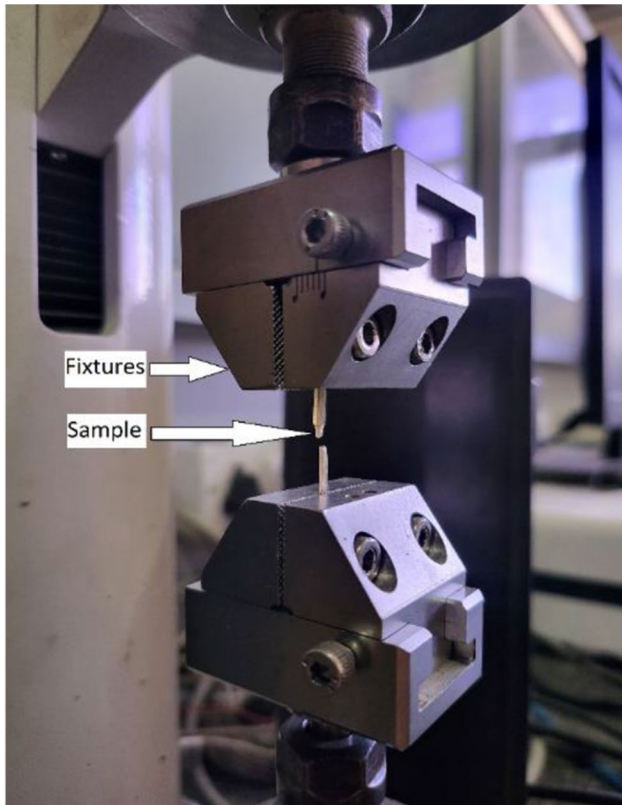


Fig. 3 Tensile specimen jogged in UTM

polymer chain and lowering the average molecular weight of the polymer. Due to this, the recycled PETG flow rate

Fig. 4 FTIR of virgin and recycled PETG

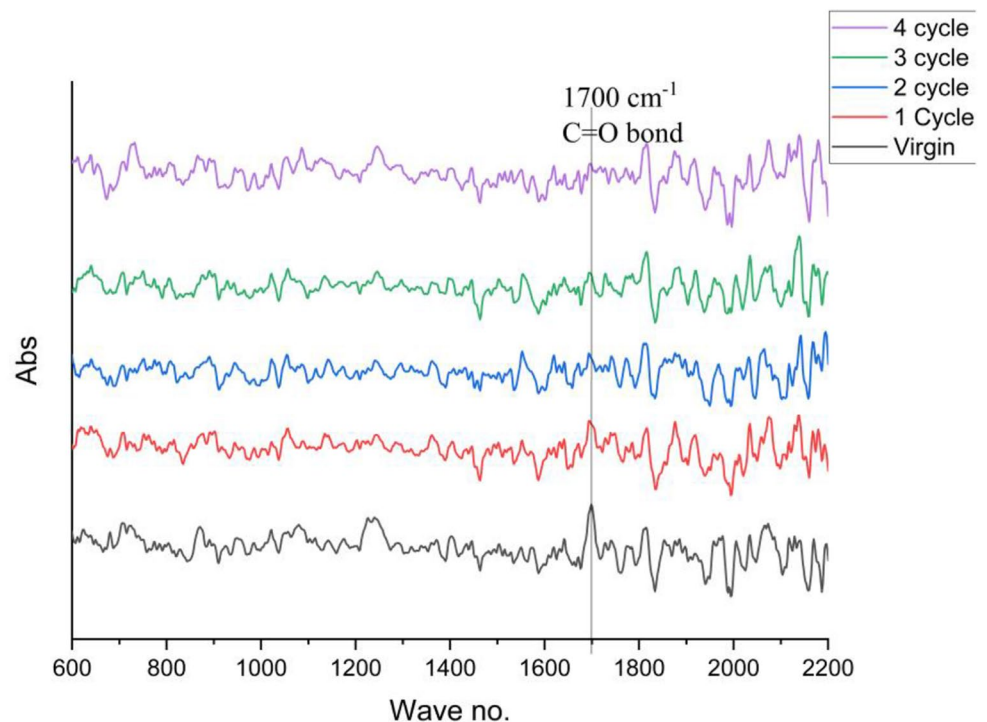


Table 1 MFI observations for virgin and recycled PETG

S.No.	Sample	Reading 1 (g/10min)	Reading 2 (g/10min)	Avg. (g/10 min)
1	Virgin	16.4	17.4	16.90
2	Cycle 1	21.18	25.9	23.54
3	Cycle 2	43.49	47.88	45.68
4	Cycle 3	48.22	47.9	48.06
5	Cycle 4	48	49	48.5

was improved. The recycling was only explored for up to 4 cycles because stagnation in MFI values was observed.

The FTIR analysis (Fig. 4) shows the peak at 1700 cm^{-1} represents the C=O bond [2]. The intensity of this bond, represented by the peak's height, is decreasing continuously from virgin to recycled PETG. The C-H bond of the cyclo-hexylene ring at 950 cm^{-1} does not show any effect of recycling on it. There is no specific variation in the intensity of the $\text{-CH}_2\text{-}$ bond at 1410 cm^{-1} [4] and peaks at 1600 cm^{-1} , 1575 cm^{-1} , 1500 cm^{-1} , and 1450 cm^{-1} which is associated with stretching of the C-C bond in benzene rings [19]. The FTIR analysis has been used to identify the type of molecule from its signature wavenumber absorbance, and it does not exhibit any relation with any physical property of the material. As observed from Fig. 4, the continuous decrease in the peak of the C=O bond and the corresponding absorbance value may be used for sensing capabilities by relating the change in resistance/ capacitance and the dielectric property of the substrate material.

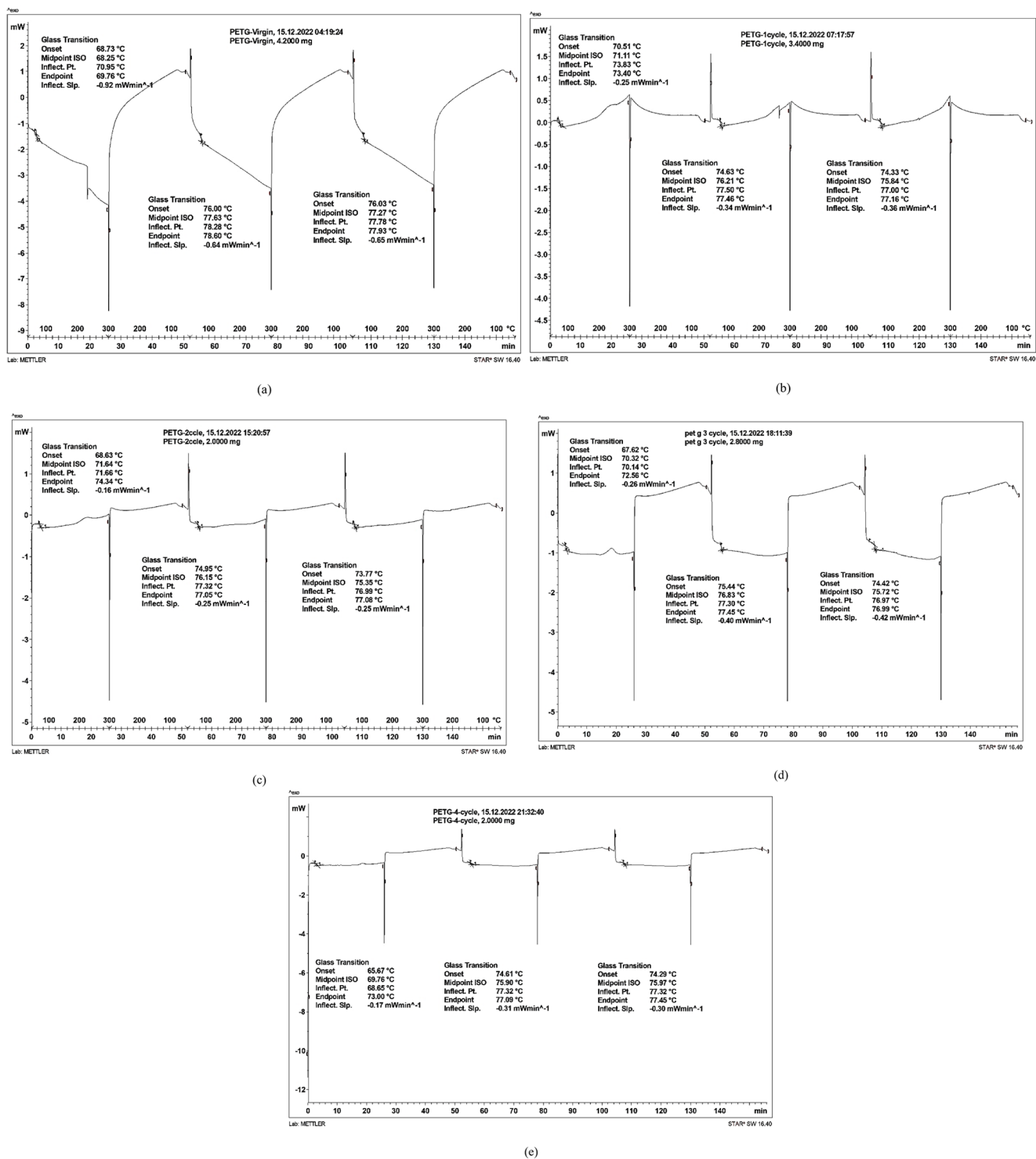


Fig. 5 DSC analysis of PETG virgin (a), cycle 1 (b), cycle 2 (c), cycle 3 (d), and cycle 4 (e)

Table 2 Tg of virgin and recycled PETG

S.No.	PETG samples	Tg (°C)
1	Virgin	77.27
2	Cycle 1	75.84
3	Cycle 2	75.35
4	Cycle 3	75.72
5	Cycle 4	75.97

Further, to ascertain the sensor applications in the temperature range of 50–75 °C, a DSC analysis was performed (Fig. 5).

As observed in Fig. 5, only one peak, i.e., of Tg, was noticed because of the amorphous nature of PETG [19]. The Tg of the recycled PETG displays a slightly lower value

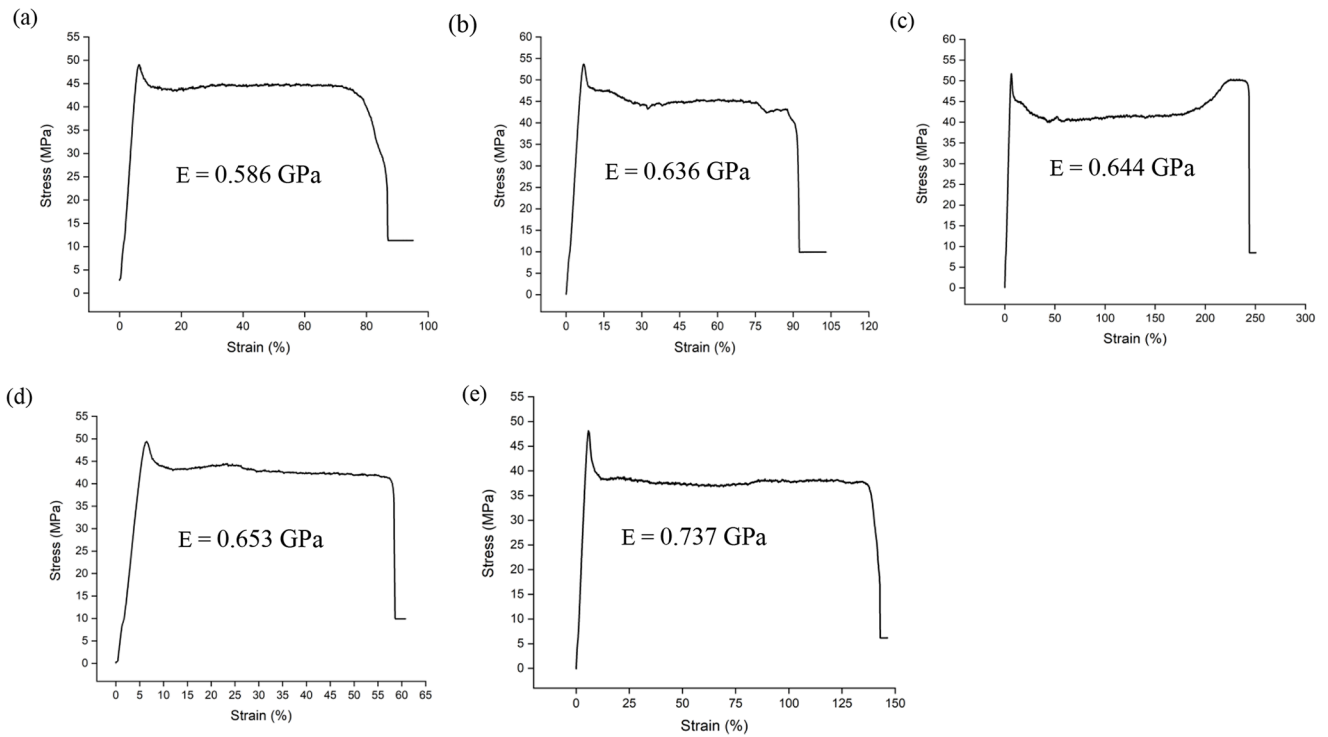


Fig. 6 Stress-Strain plots of samples prepared from virgin (a), cycle 1 (b), cycle 2 (c), cycle 3 (d), and cycle 4 (e) processed PETG

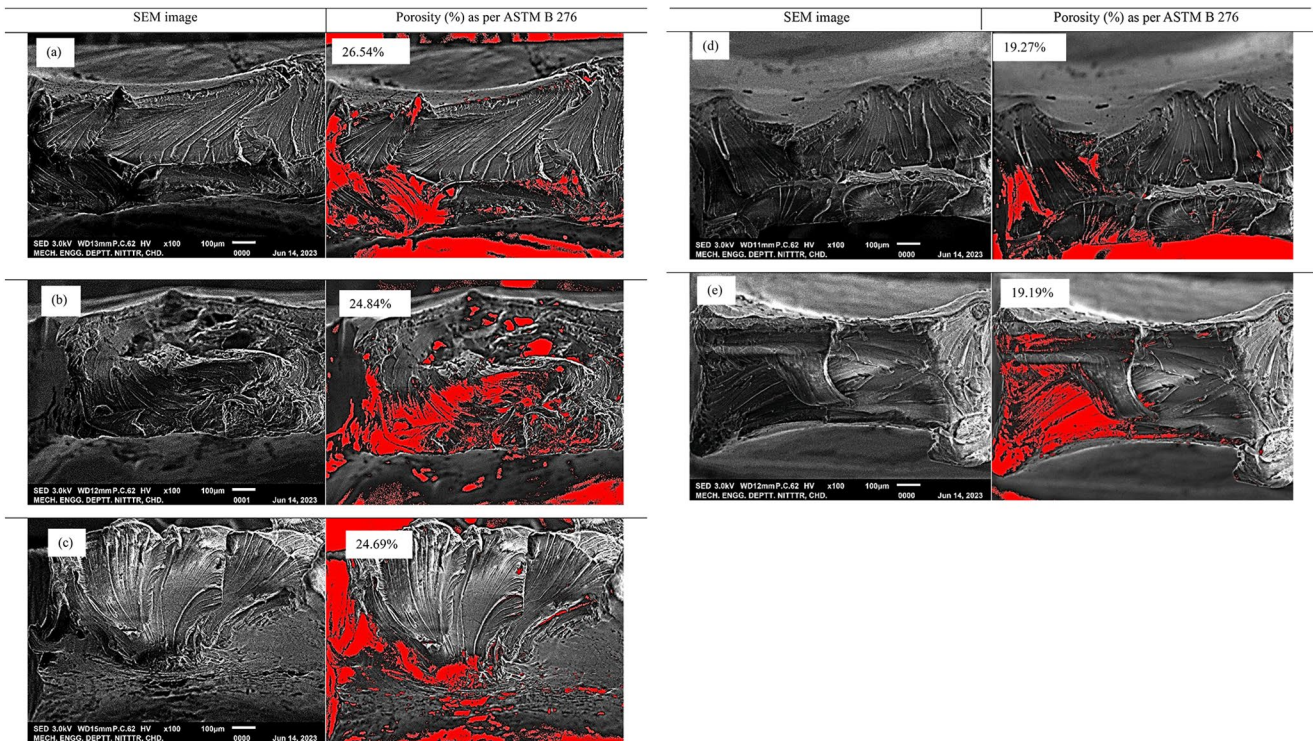


Fig. 7 SEM and porosity (%) of the processed PETG samples virgin (a), cycle 1 (b), cycle 2 (c), cycle 3 (d), and cycle 4 (e)

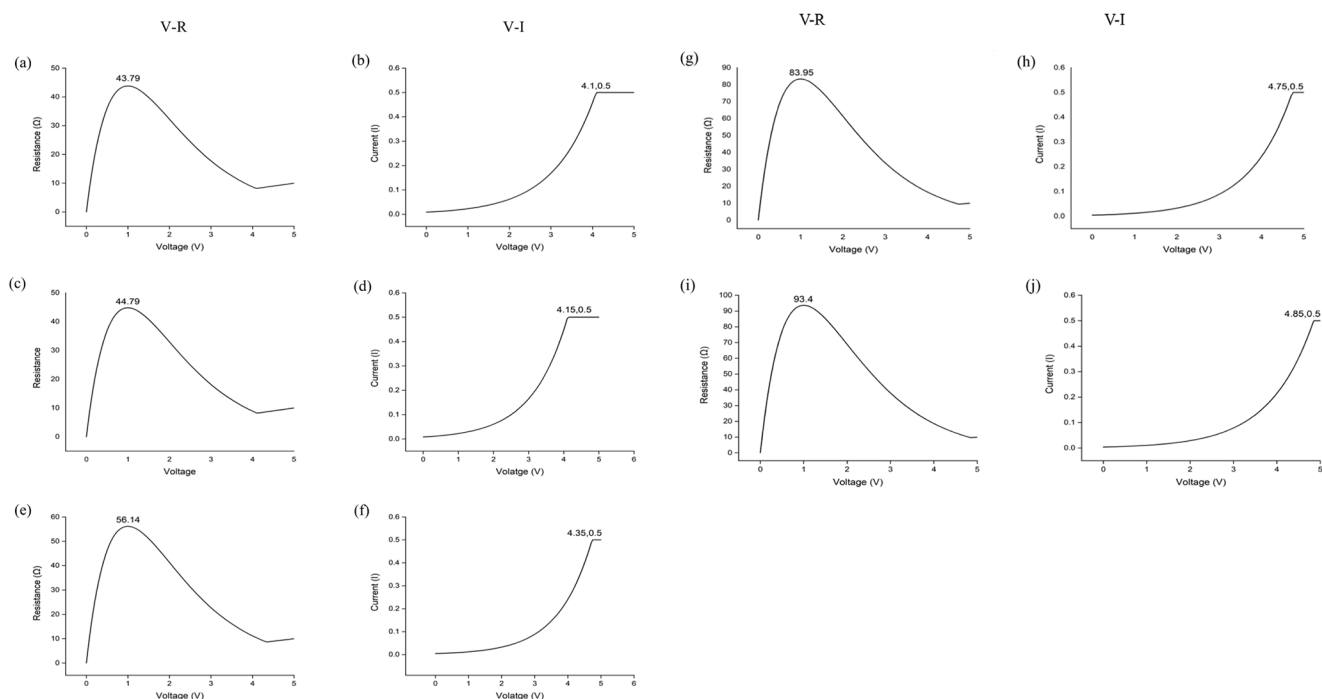


Fig. 8 V-R and V-I plots of processed PETG virgin (a, b), cycle 1 (c, d), cycle 2 (e, f), cycle 3 (g, h), and cycle 4 (i, j)

Table 3 Comparison of E, porosity (%), MFI, resistance, tg, and value of absorbance of the virgin, cycle 1, cycle 2, cycle 3, and cycle four processed PETG samples

S.No.	Sample	E (GPa)	Porosity (%)	MFI (g/10 min)	Resistance (Ω)	Voltage (V)	Tg ($^{\circ}$ C)	FTIR absorbance of C=O
1	Virgin	0.586	26.54	16.90	43.79	4.10	77.27	0.0298
2	Cycle 1	0.636	24.84	23.54	44.79	4.15	75.84	0.0165
3	Cycle 2	0.644	24.69	45.68	56.14	4.35	75.35	0.0128
4	Cycle 3	0.653	19.27	48.06	83.95	4.75	75.72	0.0107
5	Cycle 4	0.737	19.19	48.50	93.4	4.85	75.97	0.0091

than the virgin samples, which implies that the polymer might have undergone plasticization [19]. Then, for recycled PETG, the Tg remains constant due to the homogeneity of PETG and the lack of involvement of any solvent while recycling [15]. The single peak of Tg is also evidence of the purity of the material [22, 23]. Based on Fig. 5, the consolidated data is shown in Table 2.

Figure 6 shows the stress-strain plots of samples prepared from virgin, cycle 1, cycle 2, cycle 3, and cycle 4 processed PETG, which shows continuous improvement in E.

Figure 7 shows the SEM ($\times 100$) and corresponding porosity images of the fractured site of samples after testing on UTM. The increase in the E (Fig. 6) is closely related to the decreased porosity (Fig. 7) of the PETG samples at the fracture site because the pores create the stress concentration points in the material, leading to localized strain and decreasing the E. Both E and porosity are in inverse relation, which aligns with previously reported studies [24].

Finally, for sensor applications, V-R and V-I plots have been developed to understand the effect of recycling on the resistance/charge-carrying capacity of the substrate material (Fig. 8).

As observed from Fig. 8, the samples' resistance continuously increased from 43.79 Ω to 93.4 Ω for a virgin to cycle 4 PETG, respectively. In other words, the material resistance increases as the number of processing cycles increases. Hence, PETG recycling will restrict the flow of electric charge to move the same amount of charge through the 1-volt potential difference; more power is required. So, a higher voltage is needed to move 0.5 amp of current (Fig. 8). This is due to the increasing amorphous nature of PETG with recycling in line with the observed rheological property (Table 1). As the MFI of PETG increases with different processing cycles, polymer chains may go out of fashion and get misaligned, and the amorphous nature increases. With the rise in amorphous nature, restriction to the electron

flow increases, and the resistance of PETG increases in line with a previous study [25]. Based on different mechanical, rheological, morphological, thermal, and FTIR analyses, the overall comparison is shown in Table 3.

Conclusions

- PETG was mechanically recycled in this study, and its E was analyzed. The value of E increased by 42.8% (from 0.586 GPa to 0.737 GPa) as it was recycled due to the decrease in the porosity of recycled material. For the charge-carrying capacity analysis, the resistance of the samples has been evaluated. It has been observed that the resistance to recycling continuously increases. The resistance of cycle 4 PETG has risen by 113.29% compared to virgin PETG. The MFI of the material after cycle four has increased by 186.98% compared to virgin PETG. As the MFI increased, dis-ordered short polymer chains were formed, and the material became more amorphous. Due to the increase in the amorphous nature, a resistance to the electron flow occurs.
- Recycling does not affect the thermal stability of PETG as there is no considerable change in its T_g. In FTIR analysis, it has been observed that no specific variation in the absorption intensity of bonds of PETG at $WN\ 950\ \text{cm}^{-1}$, $1410\ \text{cm}^{-1}$, $1600\ \text{cm}^{-1}$, $1575\ \text{cm}^{-1}$, $1500\ \text{cm}^{-1}$, and $1450\ \text{cm}^{-1}$ were noticed except the C=O bond at $1700\ \text{cm}^{-1}$. The absorption intensity of the C=O bond decreased continuously from virgin to cycle 4 PETG.
- For sensor applications, as the resistance increases with recyclability, more energy is required to move a specific amount of charge through 1 V of potential difference, or a high potential difference is needed to pass the same amount of current, i.e., 0.5 Amp. Threshold energy also increases as the number of recyclables increases. Hence, the recycling of PETG material may be restricted to the four cycles for sensing applications in the case of the samples used in the present study.

Further studies may be performed to ascertain the effect of secondary, tertiary and quarternary recycling methods on overcoming the limitations observed after 04 recycling cycles in the present study.

Acknowledgements The authors acknowledge the research support provided by the National Institute of Technical Teachers Training and Research, Chandigarh, and Panjab University, Chandigarh. The authors thank the Department of Science and Technology for funding under FIST Level-0, Project No. SR/FST/College-/2020/997.

Competing Interests Authors do not have any competing interests.

References

1. S. Guessasma, S. Belhabib, H. Nouri, Printability and tensile performance of 3D printed polyethylene terephthalate glycol using fused deposition modelling. *Polymers*. **11**(7), 1220 (2019)
2. K. Singh, R. Singh, A.P. Singh, 3D-printed PETG-based Smart Containers for Online Health Monitoring of Food Articles. *NAS Lett.* **46**(2), 113–116 (2023)
3. P. Petrov, D. Agzamova, V. Pustovalov, E. Zhikhareva, B. Saprykin, I. Chmutin, N. Shmakova, Research into the effect of the 3D-printing mode on changing the properties of PETG transparent plastic, 24th International Conference on Material Forming, Liège, Belgique, 2021, <https://doi.org/10.25518/esaform21.3763>
4. S. Paszkiewicz, A. Szymczyk, D. Pawlikowska, I. Irska, I. Taraghi, R. Pilawka, J. Gu, X. Li, Y. Tu, E. Piesowicz, Synthesis and characterization of poly (ethylene terephthalate-co-1, 4-cyclohexanedimethylene terephthalate)-block-poly (tetramethylene oxide) copolymers, *RSC adv.*, 2017, **7**(66), p 41745–41754
5. C. Habel, M. Schöttle, M. Daab, N.J. Eichstaedt, D. Wagner, H. Bakhshi, S. Agarwal, M.A. Horn, J. Breu, B.F. High-Barrier, Packaging, *Macromol. Mater. Eng.* **303**(10), 18003331–18003335 (2018)
6. P. Baldowska-Witos, W. Kruszelnicka, A. Tomporowski, Life cycle assessment of beverage bottles, *J. Phys. Conf. Ser.* **1426**(1), 012038 (1–9) (2020)
7. K. Durgashyam, M.I. Reddy, A. Balakrishna, K. Satyanarayana, Experimental investigation on mechanical properties of PETG material processed by fused deposition modeling method. *Mater. Today Proc.* **18**, 2052–2059 (2019)
8. M.S. Srinidhi, R. Soundararajan, K.S. Satishkumar, S. Suresh, Enhancing the FDM infill pattern outcomes of mechanical behavior for as-built and annealed PETG and CFPETG composites parts, *Mater. Today Proc.* **45**(7), 7208–7212 (2021)
9. T. Balint, J. Živčák, R. Hudák, T. Tóth, M. Kohan, S. Lancoš, Destructive and non-destructive testing of samples from PLA and PETG materials. *Mater. Sci. Eng.* **1199**(1), 0120451–0120411 (2021)
10. S. Sölmann, A. Rattenholl, H. Blattner, G. Ehrmann, F. Gudermann, D. Lütkemeyer, A. Ehrmann, Mammalian cell adhesion on different 3D printed polymers with varying sterilization methods and acidic treatment. *AIMS Bioeng.* **8**(1), 25–35 (2021). <https://doi.org/10.3934/bioeng.2021004>
11. J.P. Davim, *Green Composites: Materials, Manufacturing and Engineering* (De Gruyter, Berlin, Boston, 2017). <https://doi.org/10.1515/9783110435788>
12. M. Kolli, J.P. Davim, R. Waste, Composites, Berlin, Boston: De Gruyter, 2023. <https://doi.org/10.1515/9783110766523>
13. P. Juan, R. Antonio, J.P. Davim, *Handbooks in Advanced Manufacturing, Additive Manufacturing* (Elsevier, 2021). <https://doi.org/10.1016/B978-0-12-818411-0.12001-4>
14. J.P. Davim, M. Modern, S. Engineering, Berlin, Heidelberg, 2014, <https://doi.org/10.1007/978-3-642-45176-8>
15. J.P. Davim, Introduction to Mechanical Engineering, 2018, <https://doi.org/10.1007/978-3-319-78488-5>
16. R. Singh, B.P. Singh, A.P. Singh, V. Kumar, R. Kumar, M. Bodaghi, A. Serjouei, Y. Wei, On 3D printing of low-cost sensors using recycled PET, *Sādhanā*, 2022, **47**(4), p 260
17. M. Bustos Seibert, G.A. Mazzei Capote, M. Gruber, W. Volk, T.A. Osswald, Manufacturing of a PET filament from recycled material for material extrusion (MEX), recycling, 2022, **7**, p 1–20
18. J.D. Reinaldo, M.C. Nascimento, E.N. Ito, E. Hage Junior, Rheological, mechanical and morphological properties of poly (methyl methacrylate)/poly (ethylene terephthalate) blend with dual reactive interfacial compatibilization, *Polímeros*. 2015, **25**, p 451–460

19. P. Latko-Durałek, K. Dydek, A. Boczkowska, Thermal, Rheological and Mechanical properties of PETG/rPETG blends. *J. Poly Environ.* **27**(11), 2600–2606 (2019)
20. K. Samir, G. Geoffrey, A. Samir, A. Sebastien, Investigation of 3D Printing Strategy on the mechanical performance of coextruded continuous carbon fibre reinforced PETG. *Appl. poly sci.* **138**(37), 1–15 (2021)
21. A.B. Nandiyanto, R. Oktiani, R. Ragadhita, How to read and interpret FTIR spectroscopy of organic material. *Indonesian J. Sci. Tech.* **4**(1), 97–118 (2019)
22. G. Issayev, A. Aitmagambet, E. Shehab, M.H. Ali, Bonding strength analysis of multi-material and multi-color specimens printed with multi-extrusion printer. *Manu Tech.* **21**(5), 627–633 (2021)
23. P. Franciszczyk, E. Piesowicz, K. Kalniņš, Manufacturing and properties of r-PETG/PET fibre composite – novel approach for recycling of PETG plastic scrap into engineering compound for injection moulding. *Compos. B Eng.* **154**, 430–438 (2018)
24. A. Özen, B.E. Abali, C. Völlmecke, J. Gerstel, D. Auhl, Exploring the role of manufacturing parameters on microstructure and mechanical properties in fused deposition modeling (FDM) using PETG. *App Comp. Mater.* **28**(6), 1799–1828 (2021)
25. C.S. Feng, T.W. Lu, T.L. Wang, M.Z. Lin, J. Hou, W. Lu, W.B. Liao, A novel high-entropy amorphous thin film with high electrical resistivity and outstanding corrosion resistance. *Acta Metall. Sin.* **34**(11), 1537–1545 (2021)

Publisher's Note Springer Nature remains neutral with regard to jurisdictional claims in published maps and institutional affiliations.

Springer Nature or its licensor (e.g. a society or other partner) holds exclusive rights to this article under a publishing agreement with the author(s) or other rightsholder(s); author self-archiving of the accepted manuscript version of this article is solely governed by the terms of such publishing agreement and applicable law.